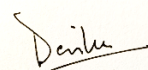


Declaration

I hereby declare that the work presented in this Thesis titled *Advanced Functional Nanomaterials for Energy and Environmental Applications* submitted to the Indian Institute of Technology Jodhpur in partial fulfilment of the requirements for the award of the degree of Doctor of Philosophy, is a bonafide record of the research work carried out under the supervision of Dr. Rakesh Kumar Sharma. The contents of this thesis in full or in parts, have not been submitted to, and will not be submitted by me to, any other Institute or University in India or abroad for the award of any degree or diploma.



Devika Laishram
P15CY001

Certificate

This is to certify that the thesis titled *Advanced Functional Nanomaterials for Energy and Environmental Applications*, submitted by *Devika Laishram* (P15CY001) to the Indian Institute of Technology Jodhpur for the award of the degree of *Doctor of Philosophy*, is a bonafide record of the research work done by her under our supervision. To the best of our knowledge, the contents of this report, in full or in parts, have not been submitted to any other Institute or University for the award of any degree or diploma.



Rakesh Kumar Sharma
Ph.D. Thesis Supervisor



Ritu Gupta
Ph.D. Thesis Co-Supervisor

Acknowledgments

I would like to extend my heartiest gratitude towards my PhD supervisor, **Dr. Rakesh Kumar Sharma** for providing his undivided support and guidance throughout the various stages during the entire period of my research at IIT Jodhpur. His encouragement and enthusiasm have helped me to successfully complete my thesis by bringing out the best version of me. I highly value his trust and the confidence he has on me allowing me to make mistakes and learn from them. I am highly grateful to **Dr. Pragati R Sharma** for her constant love, support, and encouragement.

I am highly thankful to **Dr. Ritu Gupta** for her mentorship, allowing me to do better in my research work which have compounded and improved my writing skill and bench working as well. I am highly grateful to the University of Alberta, Prof. Karthik Shankar, and Dr. Pawan Kumar for hosting me and guiding me during my six months internship at the University of Alberta, Canada.

I would like to thank my Departmental Committee for their valuable suggestions and encouragement at each stage of my PhD.

I am highly indebted to Dr. Mahesh Roy, Dr. Kiran P. Shejale, and Dr. Krishnapriya for their invaluable support and encouragement.

I am highly grateful to my friends – the ones from school who stayed till now, the ones from my graduate college, and all my other friends I met along the way. You were my backbone and will always be.

I would like to thank MHRD and IIT Jodhpur for their financial support during my PhD years. I am also grateful to DST-SERB for appointing me as one of the SERB OVDF 2018 Fellow to carry out 6 months of research at UoA, Canada.

I extend heartfelt gratefulness to the CASE facility, IIT Jodhpur, MRC, MNIT Jaipur and Nanofab facility, University of Alberta for providing me valuable instrumentation facilities for characterization of samples.

I would also like to thank Department of Chemistry, IIT Jodhpur, and everyone at IIT Jodhpur – teaching, library, administrative, housekeeping, mess, banking, and canteen staffs for providing me with my needs during this tenure.

I would like to thank my family – my parents, my brothers, sisters in law and my relatives who always believed and supported me in all my decisions. I am eternally grateful to you all for your love and sacrifices. I would like to thank my nephew, Mangal Heeyai Laishram and niece, Bidyalakshmi Laishram for being born in our family and giving us unconditional love, laughter and happiness.

I would also like to thank almighty God for his kindness and grace. I dedicate this PhD to my family especially to my mother (Laishram Ongbi K Ibetombi Devi) and father (Laishram Ranjit Singh) who despite all odds and hardships endured to bring me to where I am today. I am eternally grateful to you all.

Devika Laishram
PhD Student

List of Figures

Figures	Title	Page
1.1	Photocatalytic degradation of five different industrial dyes using the synthesized hydrogen and HfO ₂ doped TiO ₂ nanomaterials.	3
1.2	Accelerated soot oxidation activity of hydrogenated HfO ₂ nanocatalysts a result of annealing under hydrogen giving rise to enlarge of pores in the synthesized nanomaterials compared to the pristine.	4
1.3	Use of sustainable local Rajasthanian clay incorporated with Ni and Co oxides for use as catalysts in soot oxidation.	5
1.4	Nitrogen doped hollow carbon nanobubbles and solid carbon spheres for use as photoanode and counter electrode in DSSC, CO ₂ capture and as a material for supercapacitor application.	6
1.5	Schematic representation of the synthesis of cesium leads halide all-inorganic perovskite.	6
3.1	(a) XRD of the material with JCPDS data (b) XRD of highest intense peak (1 0 1) denoting shift and intensity change. (c) XRF spectra of doped TiO ₂ .	12
3.2	TEM images, HR-TEM images and the SAED images of pristine TiO ₂ (a, d, g) HfO ₂ /TiO ₂ (b, e, h) and (c, f, i) H-HfO ₂ /TiO ₂ . The inset of a, b and c show the respective spherical structure.	13
3.3	(a–c) Degradation of five different dyes using TiO ₂ , HfO ₂ /TiO ₂ and H-HfO ₂ /TiO ₂ at pH 7. (d-f) show the degradation of MB dye at different pH using H-HfO ₂ /TiO ₂ . Tauc plot of TiO ₂ (g), H-TiO ₂ (h) and H-HfO ₂ /TiO ₂ (i) respectively for band gap estimation.	14
3.4	Histogram plot of TiO ₂ , HfO ₂ /TiO ₂ and H-HfO ₂ /TiO ₂ showing different degradation efficiency of respective five dyes as indicated in the inset. (f) Plot of recyclability test for MB dye using H-HfO ₂ /TiO ₂ as photocatalyst.	15
3.5	BET isotherm plots of pristine (a) TiO ₂ , (b) H-HfO ₂ /TiO ₂ , (c) H-HfO ₂ /TiO ₂ and (d) H-HfO ₂ /TiO ₂ .	16
3.6	HPLC chromatogram of MB dye before (a) and after (b) photocatalytic degradation using H-HfO ₂ /TiO ₂ as photocatalyst.	17
4.1	(a) Schematic demonstrating the synthesis of HfO ₂ solid nanosphere aggregates by sol-gel and hydrothermal methods. (b) Schematic representation of soot oxidation activity.	20
4.2	(a) XRD patterns of p-HfO ₂ nanoparticles annealed in air and H-HfO ₂ _2h, H-HfO ₂ _6h, and H-HfO ₂ _10h, (b) Plot showing peak intensity against with a 2θ shift, (c) Plot showing variation in particle size of the synthesized HfO ₂ nanoaggregates, (d) variation of strain calculated from Williamson Hall plot and inset is the difference in color of p-HfO ₂ showing white color and H-HfO ₂ with off-white color after annealing in H ₂ and (d) Williamson Hall plot of the synthesised HfO ₂ nano aggregates, the strain is found from the slope and the crystallite size from the y-intercept by linear fitting.	21
4.3	(a) TEM and HRTEM images of air annealed HfO ₂ (a, d), 2 h (b, e), and 6 h (c, f) hydrogen annealed HfO ₂ . The SAED patterns of air annealed (g) and hydrogen annealed 2h (h) and 6h (i) samples, respectively, indicating the polycrystalline nature of HfO ₂ .	22
4.4	(a) BET adsorption-desorption isotherm and pore size desorption curve for p-HfO ₂ (a, b), H-HfO ₂ _2h (c, d), H-HfO ₂ _6h (e, f), and H-HfO ₂ _10h (g, h), respectively.	22
4.5	X-ray photoelectron spectra (XPS) of Hf 4f and O 1s in (a, c) pristine and (b, d) hydrogenated HfO ₂ , respectively. The background-subtracted raw experimental data is deconvoluted for identifying the peak contributions of Hf metal and suboxides.	24
4.6	O ₂ -TPD profile and (b) desorption peak temperature for adsorbed oxygen calculated from peak for HfO ₂ nanoaggregate samples.	25
4.7	(a) TGA profiles of carbon soot/HfO ₂ mixtures (catalyst/soot ratio of 4:1) of different HfO ₂ samples annealed in air and hydrogen, % weight loss curve and inset is the derivative of weight loss function indicating oxidative peak profile. (b) Bar graph showing the T ₁₀ , T ₅₀ , and T ₉₀ temperatures in (°C) for all of the prepared samples; the values are indicated in Table 4.5. (c) Thermogravimetric analysis of pristine and hydrogenated HfO ₂ . (d) TGA data showing the weight loss curve of carbon with T ₅₀ at 746 °C. (e) Plot of Strain and catalytic activity of the synthesized nanomaterials.	27
4.8	Reusability test of the synthesized nanomaterials as catalyst, TGA plot of the as synthesized samples of HfO ₂ with and without accelerated thermal test.	27
5.1	XRD pattern of NCS and pristine clay without doping (a), XPS survey scan (b), pore size distribution (inset), and adsorption-desorption isotherm (c) and FTIR spectra (d) of the synthesized catalysts.	30

5.2	High Resolution XPS (a) C 1s of NCS catalyst, O 1s spectra (b, c) of clay and NCS catalyst, (d) Co 2p and (e) Ni 2p high resolution scan of NCS catalyst.	31
5.3	High-resolution O ₂ TPD of (a) clay and (b) NCS catalyst with its corresponding deconvoluted profile, and 1 st order derivative (c) and deconvoluted H ₂ TPR (d) thermograms of clay and NCS catalyst and (f) H ₂ TPR of Ni clay and Co clay catalyst.	33
5.4	TEM image (a, b and c) at different scale, HRTEM image (d) and IFFT image (e and f) with corresponding FFT image (f, h) of the selected area in (e), schematic representation of soot oxidation of NCS catalyst using soot (i) and soot oxidation activity of NCS (j).	34
6.1	Scheme 1. Schematic illustration of the reaction mechanism of CS and CNB formation by modified Stöber reaction. NH ₂ Atm. is NH ₂ atmosphere, where (1) Si(OR) ₄ , (2) 3D Si-polymer network, (3) Resorcinol, (4) Formaldehyde, (5) Ethylenediamine (EDA), (6) Intermediate compound of (4) and (5) and (7) After excess reaction in between (3) and (4) forms polymer framework.	36
6.2	FESEM at different magnifications of (a, b and c) CNB and (d, e and f) CS, N ₂ adsorption and desorption isotherms of (g) CNB and (h) CS with their respective pore size distribution (inset) in the range of 0.0 to 1.0 relative pressures, (i) Raman and (j) XRD spectra (scan rate 0.1°/min).	37
6.3	TEM images of group, single and HRTEM of CNB (a-c) with mesoporous shell (7 nm) and CS (d-f) with respective SAED pattern (g) and (f). (i) XPS survey spectra of CNB and CS.	38
6.4	TGA curves and FTIR spectra of CNB and CS	39
6.5	High resolution XPS spectra of N 1s (a, d), C 1s (b, e) and O 1s (c, f) spin orbits of the synthesized CNB and CS respectively.	40
6.6	CO ₂ adsorption (a) and Cycle stability (b) of both the synthesized CS and CNB at 298 K.	41
6.7	(a, b) Plot summing up the PCE of increasing loading % of CNB and CS based photoanodes with our earlier reported material (Shejale, Laishram et al. 2016, Shejale, Laishram et al. 2017) (c) UV measurement of dye loading of different photoanodes for DSSC (d, f) Device parameters of fabricated DSSCs using the synthesized nanomaterials (dye N719, 0.5 mM and active area 0.04 cm ²) – IV graphs of the synthesized CNB and CS in combination with different % ZnO doped TiO ₂ and TiO ₂ synthesized at -40 °C (e and g), Nyquist plot (i) and bode plot (j) of the best performing solar cell, (h) equivalent model circuit used in fitting.	42
6.8	(a) Tafel plot, (b) cyclic voltammetry curves at 20 mV/s scan rate, (c) Nyquist plot with its equivalent circuit diagram (inset) of dummy cell (Consists of FTO coated Pt/CS/CNB sandwiched together and filled with 150 mM electrolyte where the active area was 0.25 cm ²). Rs: series resistance, Rct, Rw: charge transfer resistance, CPE: constant phase element and (d) schematic of a symmetrical dummy cell constructed using the synthesized carbon nanomaterials and Pt.	44
6.9	(a) Cyclic voltammetry plots (0.1mM Na ₂ SO ₄ , applied voltage 0-0.8V and scan rate 100 mV/s) with inset plot shows Nyquist plot and (b) Tafel curves with inset bar graph summarizing Tafel parameters and other electrokinetic parameters (E _{corr} corrosion potential (mV), I _{corr} corrosion current (μA), β _a anodic and β _c cathodic β Tafel constant (mV) of CS and CNB, CV obtained from CS (c) and CNB (d) at various scan rates.	45
7.1	Schematic representation of the thesis overview	48
7.2	PL spectra (a) and UV-vis spectra (b) of the synthesized different CsPbBr ₃ composites. Inset (b) shows the band adsorption edge of GCN-CsPbBr ₃ at 520 nm.	49
7.3	Photographic images of pristine CsPbBr ₃ (a) under day light and under UV light (λ = 365 nm) of Sn-CsPbBr ₃ (b), Ta-CsPbBr ₃ (c), Ti-CsPbBr ₃ (d), Mo-CsPbBr ₃ (e) and GCN-CsPbBr ₃ (f) deposited on glass.	49
7.4	High resolution TEM images of Mo-CsPbBr ₃ (a) and GCN-CsPbBr ₃ (b) showing lattice fringes and d-spacing.	50
7.5	Survey scan (a) and High resolution XPS spectra of Mo-CsPbBr ₃ and GCN-CsPbBr ₃ in Cs 3d (b), Pb 4f (c), Br 3d (d) and Mo 3d (e) region.	50
7.6	High resolution XPS spectra of GCN-CsPbBr ₃ in C 1s (a), O 1s (b) and N 1s (c) region and Mo-CsPbBr ₃ in C 1s (d) and O 1s (e) region.	51
7.7	Linear sweep voltammetry (LSV) under AM1.5 G solar simulated light with and without 420 nm UV cut-off filter for GCN-CsPbBr ₃ (a) and Mo-CsPbBr ₃ (b) and LSV of Ti-CsPbBr ₃ , Ta-CsPbBr ₃ and Sn-CsPbBr ₃ without UV filter.	52
7.8	Photoelectrochemical study of GCN-CsPbBr ₃ . Current density vs applied voltage curve during an ON-OFF light cycle (a), Light On-OFF amperometric i-t curve under AM1.5G solar simulated light with and without 420 nm cut-off filter (b), Amperometric li-t curve at +0.6 V applied bias when exposed to LEDs of different wavelength at 365, 420, 460, 580 and 640	52

	nm (c), EIS Nyquist plot (d) and Mott-Schottky (e).	
7.9	Photoelectrochemical study of Mo-CsPbBr ₃ . Current density Vs voltage curve during an ON-OFF light cycle (a), Light On-OFF amperometric i-t curve under AM1.5G solar simulated light with and without 420 nm filter cut-off of (b), Amperometric i-t curve at +0.6 V applied bias when exposed to LEDs of different wavelength at 365, 420, 460, 580 and 640 nm (c), EIS Nyquist plot (d) and Mott-Schottky (e).	53
7.10	Photographic image of all inorganic perovskite CsPbBr ₃ and CsPbI ₃ demonstrating the change in photoluminescence (green to red) by changing the constituting anion.	53

...

List of Tables

Table	Title	Page
3.1	Cell parameters of the synthesized SNP.	12
3.2	Degradation activity of MB dye with different catalysts.	15
3.3	Surface area analysis of all the samples.	16
4.1	Particle size, <i>d</i> -spacing and strain calculated for the hydrogenated HfO ₂ .	21
4.2	Surface properties of HfO ₂ air, 2h, 6h and 10h from BET analysis.	23
4.3	Binding Energy of O 1s and Hf 4f Core Levels for p-HfO ₂ and H-HfO ₂ .	24
4.4	Surface oxygen species present in p-HfO ₂ , H-HfO ₂ _6h where O _{α2} , O _{α1} , and O _β % are calculated from % area under respective peaks.	24
4.5	O ₂ -TPD parameters of the synthesized catalysts	25
4.6	TGA parameters of the as-synthesized HfO ₂ and after an accelerated thermal test (ATT)	26
5.1	Properties of Catalyst from BET and O ₂ TPD.	31
6.1	Surface porosity and chemical composition of CNB and CS.	37
6.2	Distribution of the N components in the synthesized materials	40
6.3	Photovoltaic DSSC data obtained from I-V and EIS	42
6.4	Result of dye de-loading measured with UV-vis spectrometer where, ϵ is the coefficient of absorbance with 1.4×10^4 for N ₃ dye, <i>l</i> is the length of the cuvette (1 cm)	43

...

List of Symbols

Symbol	Description
α	Alpha
β	Beta
π	Pie
$C=O$	Carbonyl group
λ_{\max}	Maximum wavelength
λ_{em}	Emission wavelength
λ_{ex}	Excitation wavelength
C_{SC}	Chemical capacitance
Ω	ohm
C_T	Electrolyte capacitance
T_{10}	Onset temperature
T_{50}	Light off temperature
T_{90}	Maximal conversion temperature
T_m	Peak temperature
$-NH_2$	Amino group
T_m	Melting temperature
T_{10}	The temperature at which 10% of the total weight loss occurs
T_{50}	Light off temperature at which 50% of the total weight loss occurs
T_{90}	The temperature at which 90% of the total weight loss occurs
μM	Micrometers
mM	Millimeter
nm	Nanometer
$-OH$	Hydroxyl group
$-O-CH_3$	Methoxy group
cm	Centimeters
$^{\circ}\text{C}$	Degree celsius
J_0	Exchange current density
J_{lim}	Limiting current density
E_{pp}	Peak to peak potential
O_{β}	Lattice oxygen
O_{α}	Chemisorbed oxygen
N_3	Ruthenium based dye
τ	Lifetime
HCl	Hydrogen chloride
n	Binding parameter
μL	Microliters
Hz	Hertz
V	Voltage
CaCl_2	Calcium chloride
KOH	Potassium hydroxide
R_s	Series resistance
R_{ct}	Charge transport resistance
V_{OC}	Open circuit Potential
J_{sc}	Short circuit potential
F	farad
R_1, R_2	Counter electrode and electrolyte charge transfer resistance

...

List of Abbreviations

AIP	All-inorganic perovskite
ALD	Atomic Layer Deposition
AM	Air Mass
a.u.	Arbitrary Unit
B.E.	Binding Energy
BET	Brauner Emmett Teller
BJH	Barrett Joyner Halenda
CE	Counter Electrode
CN	Carbon nitride
CNB	Carbon nanobubble
CNT	Carbon Nanotube
CPE	Constant Phase Element
CR	Cresol Red
CS	Carbon sphere
CV	Cyclic Voltammetry
DI	De-ionized
DRS	Diffuse Reflectance Spectra
DSSC	Dye-Sensitized Solar Cells
EIS	Electrochemical Impedance Spectroscopy
FCC	Face Centered Cubic
FE-SEM	Field Emission Scanning Electron Microscope
FF	Fill Factor
FWHM	Full Width Half Maximum
FTO	Fluorine Doped Tin Oxide
g-C ₃ N ₄	Graphitic carbon nitride
GCN	Graphitic Carbon nitride
GW	Gigawatt
HIP	Hafnium isopropoxide
HDA	Hexadecylamine
HOMO	Highest Occupied Molecular Orbital
HR-TEM	High Resolution Transmission Electron Microscope
ICDD	International Centre for Diffraction Data
JCPDS	Joint Committee on Powder Diffraction Standards
LHE	Light Harvesting Efficiency
LUMO	Lowest Unoccupied Molecular Orbital
MB	Methylene blue
MO	Methyl orange
MWCNT	Multi-walled Carbon Nanotube
NBE	Near Band Edge
NCs	Nanocrystals
NIR	Near-Infrared
OA	Oleic Acid
OAm	Oleylamine
ODE	1-octadecene
PCE	Photo Conversion Efficiency
PL	Photoluminescence Spectroscopy
PV	Photovoltaic
rpm	Revolution per minute
SAED	Selected Area Electron Diffraction
SB	Solochrome black
SNP	Nanospheroids
TTIP	Titanium tetra isopropoxide
TB	Thymol blue
TPD	Temperature Programmed Desorption
TPO/R	Temperature Programmed Oxidation/Reduction
TW	Terra watt

UV-vis *Ultraviolet-Visible Spectroscopy*
XRD *X-ray Diffraction*
XPS *X-ray Photoelectron Spectroscopy*